Supplementary Information (SI) for Inorganic Chemistry Frontiers.
This journal is © the Partner Organisations 2025

Supplementary information

Gas/solid/liquid triphase interface of carbon nitride for efficient photocatalytic H_2O_2 production

Mao He, Xiaoying Peng, Suqin Wu,* Bin Lei, Shuai Xiong, Qin Luo, Zongxing Tu, Xiaoxue Lin, Guiming Peng*

College of Chemistry and Materials, National Engineering Research Center for Carbonhydrate Synthesis, Key Lab of Fluorine and Silicon for Energy Materials and Chemistry of Ministry of Education, Key Laboratory of Green Catalysis of Jiangxi Education Institutes, Jiangxi Normal University, Nanchang 330022, China

E-mail: 090250@jxnu.edu.cn (S. W.), guiming@jxnu.edu.cn (G. P.)

Experimental Procedures

Synthesis of CN and PABA/CN:

Synthesis of pristine CN: Typically, 5 g of melamine in a closed crucible was heated to 550 °C at a ramp rate of 5 °C/minute in a muffle furnace in air atmosphere. The system was kept at 550 °C for 4 hours. After cooling down naturally, the bulk CN was obtained.

Synthesis of PABA/CN: 4-aminobenzoyl groups were grafted onto CN surface by the thermal vapor-assisted method. Specifically, 0.05 g 4-aminobenzoic acid was placed at the bottom of a quartz tube, while 0.1 g pristine CN was placed in the middle of the tube. After closing the tube with aluminum foil, it was transferred to a tube furnace. Then the system was heated to 300 °C at a ramp rate of 5 °C/min in N_2 atmosphere and maintained at 300 °C for 1 hour. After cooling down, the CN modified with 4-aminobenzoyl groups was obtained (PABA/CN). As a control, the CN-300 powder was obtained following the same procedures as above but without 4-aminobenzoic acid.

Photocatalytic H_2O_2 production：

3 mg catalyst was dispersed in 30 mL deionized water by sonication in a quartz photocatalytic reactor (100 mL). Then O_2 was bubbled into the system in dark condition for 30 minutes to achieve an adsorption-desorption equilibrium. Photocatalytic H_2O_2 production was performed under illumination of Xe lamp (CEL-HXUV300E-T3, China Education Au-light) coupled with the 350-780 nm filter at the power intensity of 2-SUN. O_2 was continuously bubbled into the system while the temperature was kept at 25 ± 0.5 °C using a water-cooling system. H_2O_2 productions at different wavelengths were performed following the same procedures but with specific 400, 420, 450, 475, and 500 nm filters.

The concentration of H_2O_2 was determined using the horseradish peroxidase/ 3,3',5,5'-tetramethylbenzidine (HRP/TMB) colorimetric method with a UV-vis spectrophotometer. Typically, 0.2 mL of the reaction solution was mixed with 1 mL of solution which contains acetate buffer (0.1 M, pH 3.5), TMB (100 μmol/L), and HRP

(50 μg/mL). The mixture was left in the dark for 5 minutes. Then the colorless TMB reacts with H_2O_2 in the presence of HRP to form the blue TMB-Ox product. The concentration of H_2O_2 was determined according to the UV-vis absorbance of TMB-Ox at 652 nm calibrated by the standard H_2O_2 concentration-absorbance plot.

H_2O_2 decomposition and formation constants test:

Due to the simultaneous formation and self-decomposition of H_2O_2 during the photocatalytic process, the H_2O_2 decomposition and formation constants are acquired following the below widely used equation[1]: $[H_2O_2] = (K_f / K_d) \{1- exp(-K_d t)\}$ where $[H_2O_2]$, K_f, and K_d represent the concentration of H_2O_2, formation constant and decomposition constant, respectively.

Electrochemical measurements:

Rotating ring-disk electrode (RRDE) measurements were conducted by a standard three electrodes connected to the potentiostat (CHI 760E). An Ag/AgCl electrode and Pt foil (1 cm × 1 cm) were used as reference electrode and counter electrode, respectively. To prepare the working electrode, 1 mg of catalysts and 20 μL Nafion were dispersed in 1.98 mL ethanol solution to form 2 mL homogeneous solution. Then 10 μL of the above suspension was evenly dropped onto a clean glassy carbon electrode, and was dried before use. The LSV curves were recorded in O_2-saturated 0.1 M phosphate buffer solution (pH = 6.9) with the scan rate of 5 mV/s at different rotating speeds of 400, 800, 1200 and 1600 rpm. The electron transfer number (n) of ORR for H_2O_2 production was obtained by two methods. (i) Electron transfer number and selectivity of H_2O_2 production could be obtained from the relation between disk current and ring current (mA). Specifically, they can be calculated from the below equation:

$$n = 4\times(I_d \cdot N)/(I_d \cdot N+I_r)$$

$$H_2O_2\% = 200 \times I_r/(N\, I_d+I_r)$$

where I_d is the disk current, I_r is the ring current and N is the collection efficiency. The collection efficiency "*N*" was experimentally determined to be 0.36 by a standard ferricyanide system.

(ii) Electron transfer number was also obtained by the Koutecky-Levich (K-L)

equation based on LSV curves at different rotating speeds: $j^{-1} = j_k^{-1} + B^{-1}\,\omega^{-1/2}$, $B = 0.2nFC_oD_o^{2/3}v^{-1/6}$. Herein, j represents current density (mA/cm^2); j_k is the kinetic current density and ω means the angular velocity (rad/s); F is Faraday constant (96485 C/mol); the v expresses dynamic viscosity of H_2O (0.01 cm^2/s); C_0 is the concentration of O_2 in water (1.1×10^{-3} mol/cm^3) and D_0 represents diffusion coefficient of O_2 (1.93×10^{-5} cm^2/s), respectively.

The transient photocurrents, Mott-Schottky plots, electrochemical impedance spectra (EIS) were tested using the same three-electrode potentiostat system (CHI 760E) but in 0.5 M Na_2SO_4 solution. For these tests, the working electrode was prepared by drop-casting the catalyst ink (5 mg catalyst in mixture of 0.98 mL ethanol and 20 µL Nafion) onto FTO surface. It was dried before use.

Material characterizations:

The morphologies of the materials were examined by scanning electron microscopy (SEM, Tescan Clara) and transmission electron microscopy (TEM, JEM2100). The X ray diffractometer (XRD) patterns were collected on a Bruker D8 Advance diffractometer (Cu Kα X-ray radiation, λ = 1.54 Å) at room temperature. The chemical compositions of the catalyst were studied by Fourier transform infrared (FTIR, Nicolet 6700) and X-ray photoelectron spectroscopy (XPS, Thermo-VV Sciential) and ^{13}C solid-state nuclear magnetic resonance (NMR, Bruker 400M). UV-vis diffuse reflectance spectra were collected on a Shimadzu UV-Vis-NIR spectrophotometer (UV-2600i). Photoluminescence (PL) spectra were recorded using a steady-state transient fluorescence spectrometer (FLS980). Moreover, the electron paramagnetic resonance (EPR) signals were recorded on Bruker A300 spectrometer. The Brunauer-Emmett-Teller (BET) method was used to obtain the specific surface areas of samples and pore-size distribution.

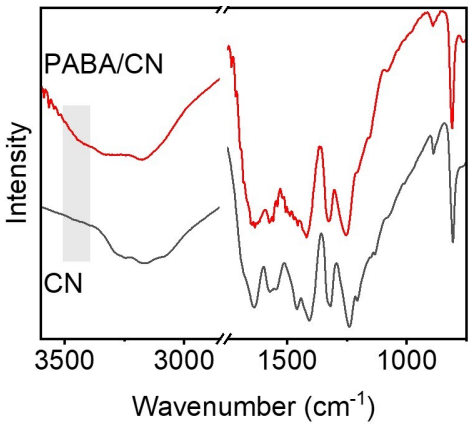

Figure S1. FTIR of CN and PABA/CN.

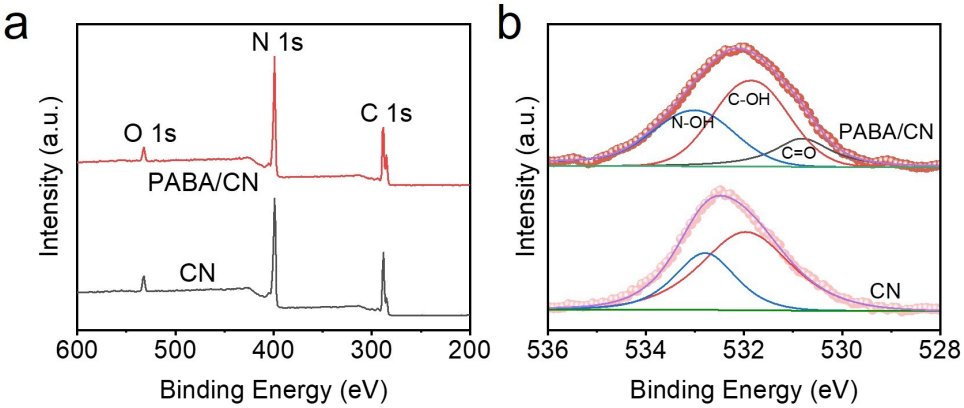

c

	O%	C%	N%	C/N
CN	5.21	44.13	50.66	0.87
PABA/CN	5.58	48.90	45.53	1.07

Figure S2. (a) XPS survey spectra, (b) O1s XPS spectra, and (c) Atomic ratios of CN and PABA/CN.

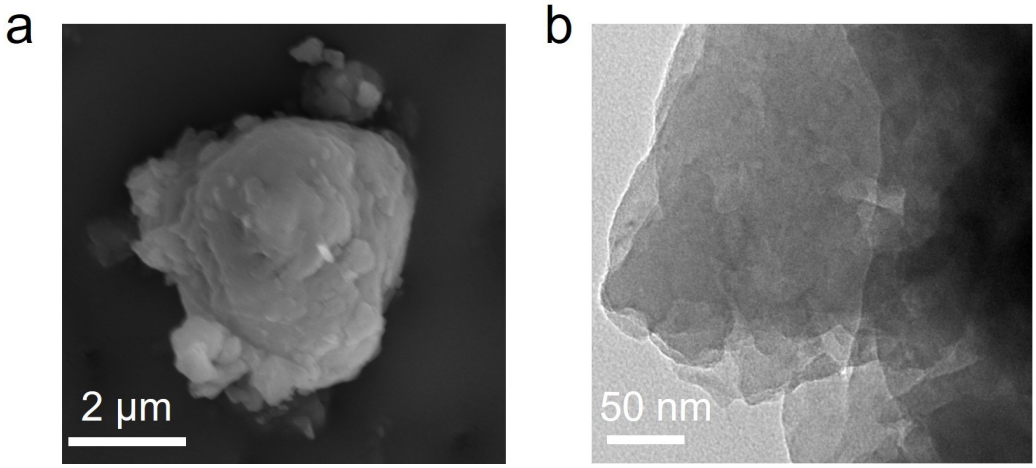

Figure S3. (a) SEM and (b) TEM image of CN.

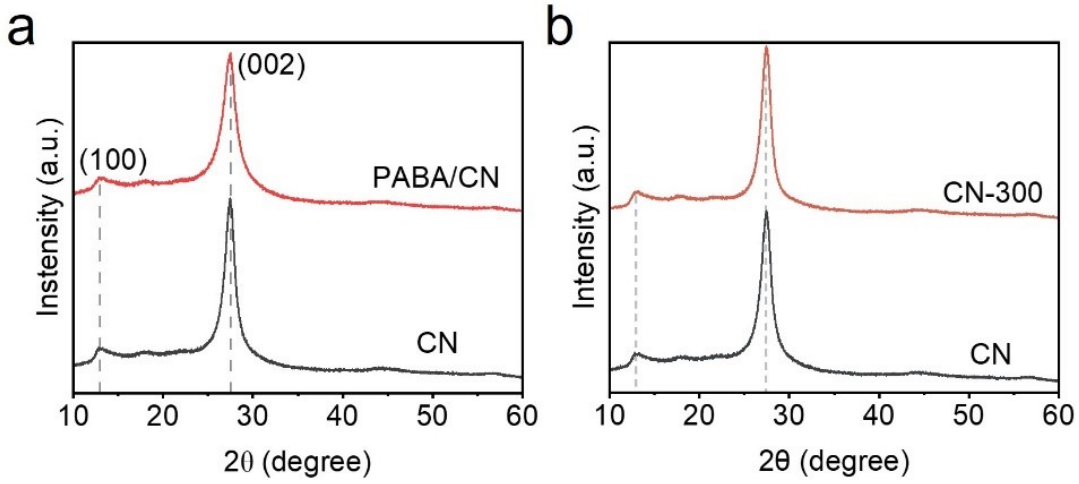

Figure S4. (a) XRD patterns of pristine CN and PABA/CN. (b) XRD patterns of CN after thermal treatment at 300 ℃.

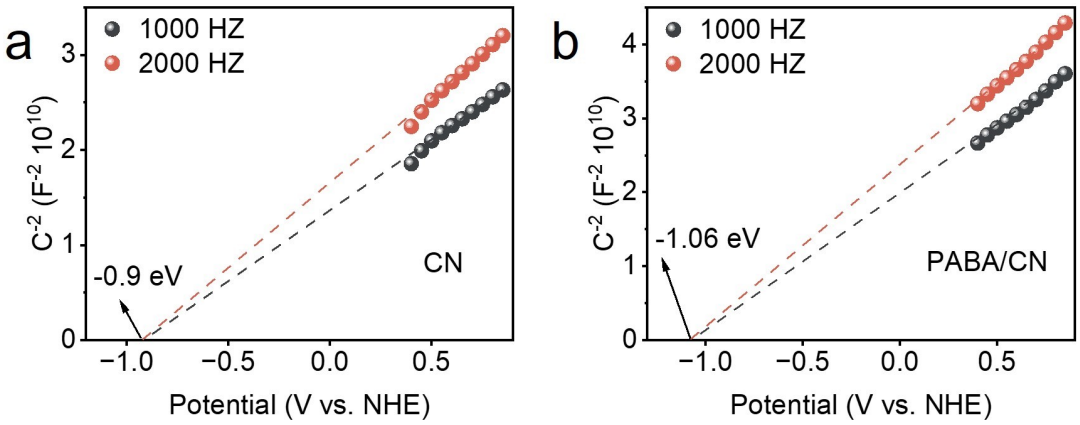

Figure S5. Mott-Schottky plots of (a) CN and (b) PABA/CN.

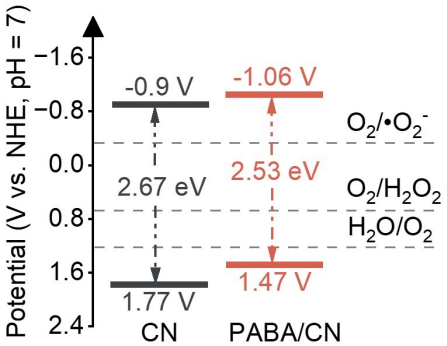

Figure S6. Bandgap diagram of CN and PABA/CN.

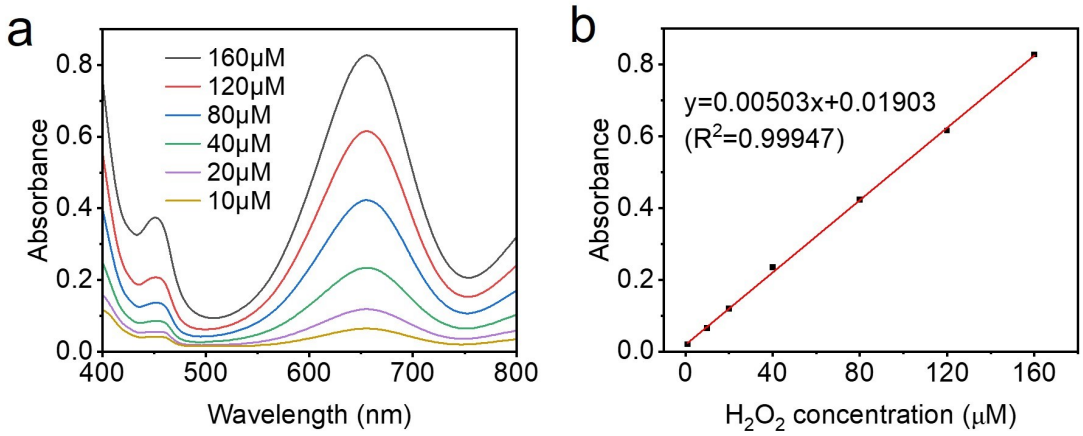

Figure S7. (a) UV-vis absorbance spectra of TMB-Ox after reaction with H_2O_2 of different concentrations and (b) corresponding linear relationship (standard plot) between the absorbance at 652 nm and H_2O_2 concentration.

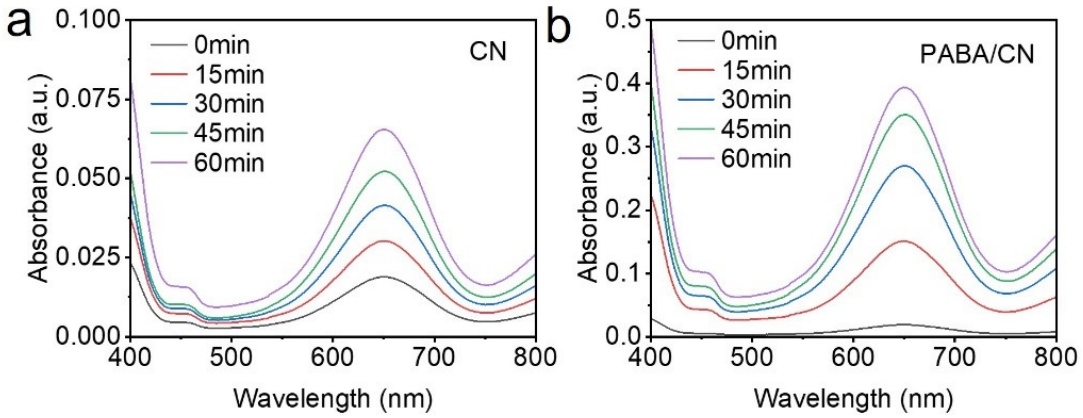

Figure S8. Time-dependent UV-vis absorption spectra for H_2O_2 production when using (a) CN and (b) PABA/CN as photocatalyst.

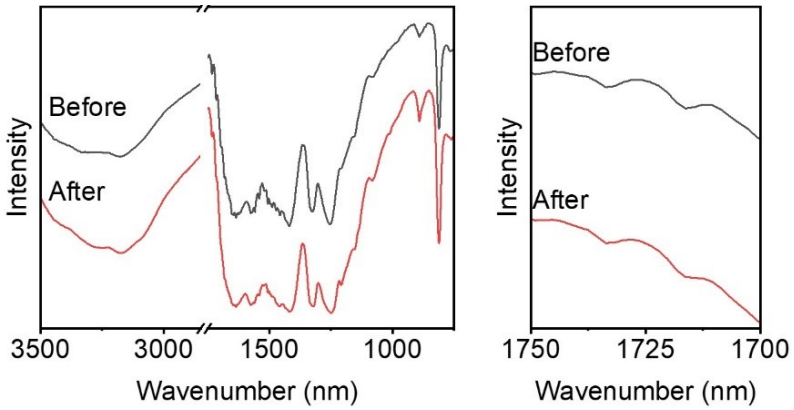

Figure S9. FITR spectra of PABA/CN before and after cycling tests.

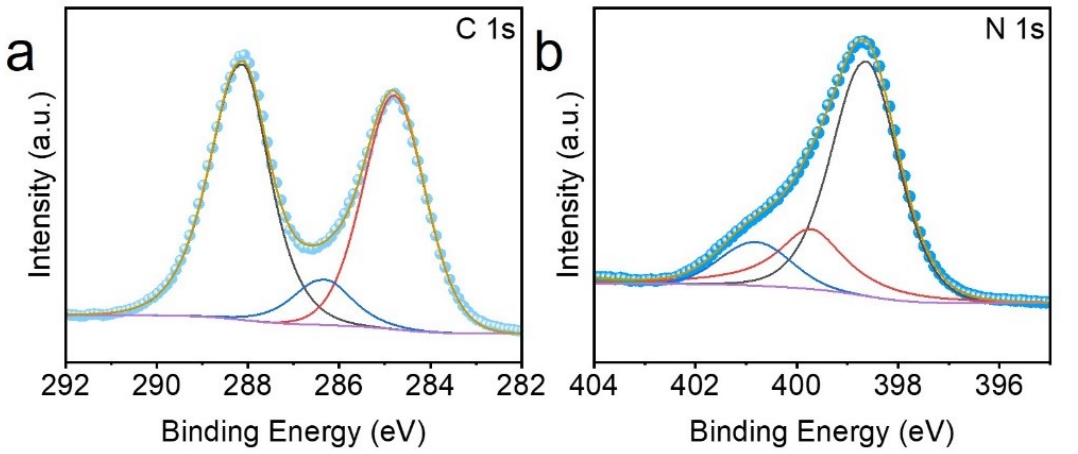

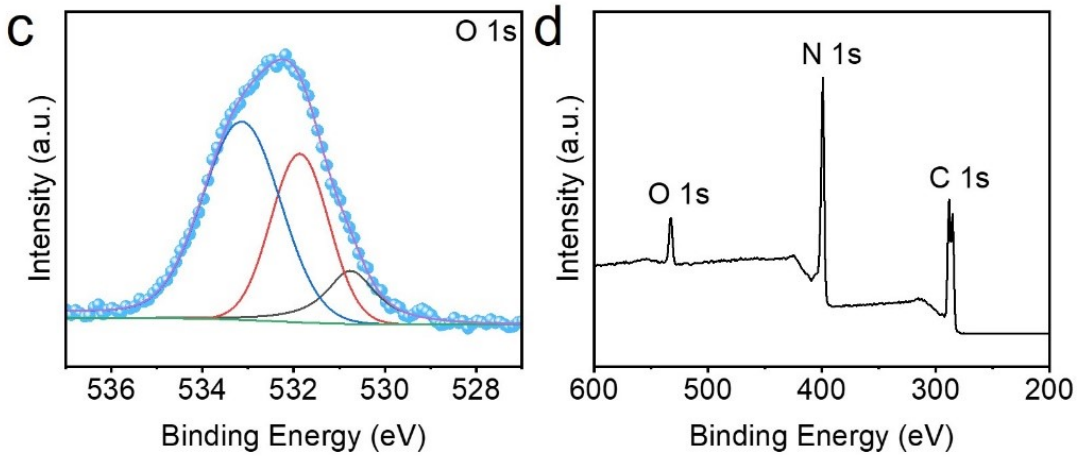

e

O%	C%	N%	C/N
1.37	49.90	48.73	1.02

Figure S10. XPS spectra of PABA/CN before and after cycling tests.

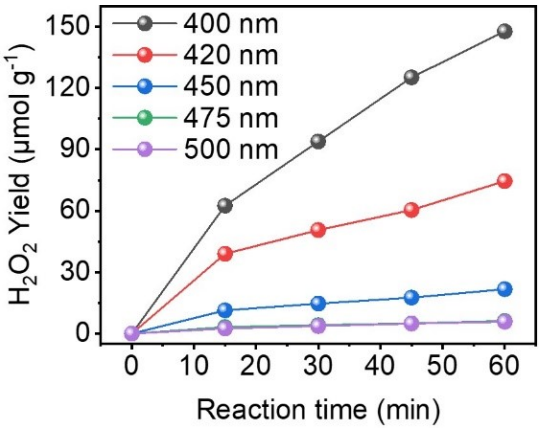

Figure S11. H_2O_2 production by PABA/CN under illumination with different wavelengths.

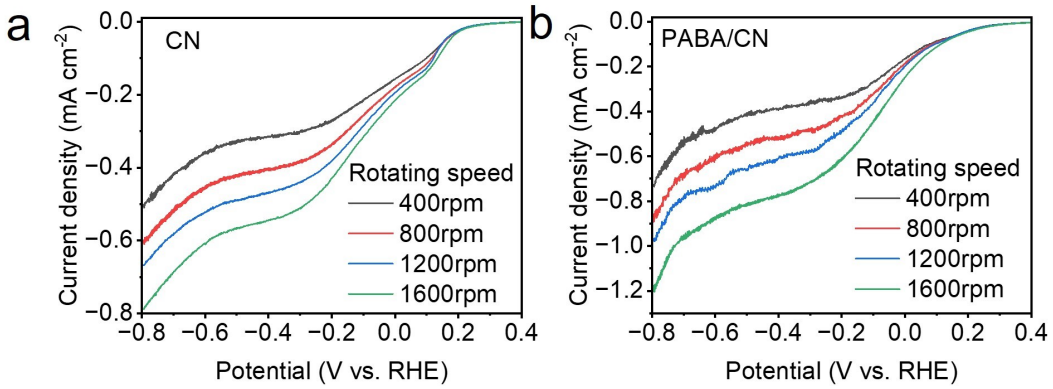

Figure S12. The LSV curves obtained at different rotating speeds. (a) CN, (b) PABA/CN.

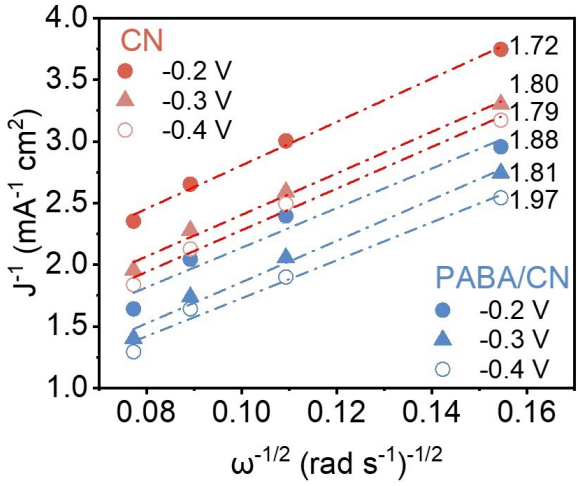

Figure S13. The Koutecky-Levich plots for CN and PABA/CN obtained from the LSV curves at different potentials.

Table S1. Representative photocatalytic H_2O_2 production performances for CN-based photocatalysts.

Photocatalysts	Sacrificial Agent	H_2O_2 (μmol g^{-1} h^{-1})	Ref.
Nv-C≡N-CN	Pure water	323	2
PEI/g-C_3N_4	Pure water	208.1	3
Co/AQ/C_3N_4	Pure water	124	4
g-C_3N_4-ND4-OM3	Pure water	146.96	5
Ag@U-g-C_3N_4	Pure water	70	6
CN/rGO@BPQDs	Pure water	60.6	7
CN(urea)	Pure water	144.4	8
Sb/PCN(10.9 wt.%)	Pure water	182.4	9
GCN	pure water	507.82	10

fl-CN-530	Pure water	952	[11]
CN/rGO@BPQDs-0.04	Pure water	60.6	[12]
Cv-PCN	Pure water	2063.21 (Triphase system)	[13]
		363.12 (Diphase system)	
ZnPPc-NBCN	10 vol% IPA	114	[14]
KCl@g-C_3N_4	10 vol% EtOH	202	[15]
ACNN	10 vol% EtOH	204	[16]
CAN-10	10 vol% IPA	174	[17]
Ti_3C_2/g-C_3N_4	10 vol% IPA	131.71	[18]
CDs_{10}MCN	10 vol% IPA	423.17	[19]
Ultra-thin g-C_3N_4	10 vol% EtOH	43	[20]
CN-MCA-U-2.5	10 vol% EtOH	377.06	[21]
6BP/CN	10 vol% IPA	501.4	[22]
BU-3	10 vol% IPA	72.3	[23]
C_3N_4-Urea	10 vol% EtOH	4900	[24]
P- C_3N_4/O- C_3N_4	10 vol% EtOH	179	[25]
6%BP/OPCN	10 vol% IPA	3463	[26]
DCN	10 vol% IPA	665.4	[27]
50PCN	10 vol% EtOH	285.3	[28]
CN-Ar	30 vol% MeOH	5775	[29]
Ni/PCN(0.52 wt.%)	10 vol% IPA	27110	[30]
AQ-CNx	10 vol% IPA	1821	[31]
PABA/CN	**Pure water**	**745.0**	**This work**
	5 vol% EtOH	**2360**	

Reference

1 Q. Chen, C. Lu, B. Ping, G. Li, J. Chen, Z. Sun, Y. Zhang, Q. Ruan and L. Tao, A hydroxyl-induced carbon nitride homojunction with functional surface for efficient photocatalytic production of H_2O_2, *Appl. Catal., B*, 2023, **324**, 122216.

2 X. Zhang, P. Ma, C. Wang, L. Gan, X. Chen, P. Zhang, Y. Wang, H. Li, L. Wang, X. Zhou and K. Zheng, Unraveling the dual defect sites in graphite carbon nitride for ultra-high photocatalytic H_2O_2 evolution, *Energy Environ. Sci.*, 2022, **15**, 830-842.

3 K. Schwinghammer, M. B. Mesch, V. Duppel, C. Ziegler, J. Senker and B. V. Lotsch, Crystalline Carbon Nitride Nanosheets for Improved Visible-Light Hydrogen Evolution, *J. Am. Chem. Soc.*, 2014, **136**, 1730-1733.

4 H. Guo, J. Raj, Z. Wang, T. Zhang, K. Wang, L. Lin, W. Hou, J. Zhang, M. Wu, J. Wu and L. Wang, Synergistic Effects of Amine Functional Groups and Enriched-Atomic-Iron Sites in Carbon Dots for Industrial-Current–Density CO_2 Electroreduction, *Small*, 2024, **20**, 2311132.

5 Y.-X. Ye, J. Pan, F. Xie, L. Gong, S. Huang, Z. Ke, F. Zhu, J. Xu and G. Ouyang, Highly efficient photosynthesis of hydrogen peroxide in ambient conditions, *Proc. Natl. Acad. Sci. U.S.A.*, 2021, **118**, e2103964118.

6 C. Chu, W. Miao, Q. Li, D. Wang, Y. Liu and S. Mao, Highly efficient photocatalytic H_2O_2 production with cyano and SnO_2 co-modified g-C_3N_4, *Chem. Eng. J.*, 2022, **428**, 132531.

7 J. Li, H. Shi, Z. Li, J. Wang, H. Si, F. Liao, H. Huang, Y. Liu and Z. Kang, Interaction of metal ions in high efficiency seawater hydrogen peroxide production by a carbon-based photocatalyst, *Appl. Catal., B*, 2024, **343**, 123541.

8 D. He, Z. Zhang, Y. Xing, Y. Zhou, H. Yang, H. Liu, J. Qu, X. Yuan, J. Guan and Y.-n. Zhang, Black phosphorus/graphitic carbon nitride: A metal-free photocatalyst for “green” photocatalytic bacterial inactivation under visible light, *Chem. Eng. J.*, 2020, **384**.

9 Z. Teng, Q. Zhang, H. Yang, K. Kato, W. Yang, Y.-R. Lu, S. Liu, C. Wang, A. Yamakata, C. Su, B. Liu and T. Ohno, Author Correction: Atomically dispersed antimony on carbon nitride for the artificial photosynthesis of hydrogen peroxide, *Nat. Catal.*, 2021, **4**, 533.

10 Y. Wu, J. Chen, H. Che, X. Gao, Y. Ao and P. Wang, Boosting $2e^-$ oxygen reduction reaction in garland carbon nitride with carbon defects for high-efficient photocatalysis-self-Fenton degradation of 2,4-dichlorophenol, *Appl. Catal., B*, 2022, **307**, 121185.

11 B. Feng, Y. Liu, K. Wan, S. Zu, Y. Pei, X. Zhang, M. Qiao, H. Li and B. Zong, Tailored Exfoliation of Polymeric Carbon Nitride for Photocatalytic H2O2 Production and CH4 Valorization Mediated by O_2 Activation, *Angew. Chem. Int. Ed.*, 2024, **63**, e202401884.

12 J. Xiong, X. Li, J. Huang, X. Gao, Z. Chen, J. Liu, H. Li, B. Kang, W. Yao and Y. Zhu, CN/rGO@BPQDs high-low junctions with stretching spatial charge separation ability for photocatalytic degradation and H_2O_2 production, *Appl. Catal., B*, 2020, **266**, 118602.

13 S. Yan, Y. Li, X. Yang, X. Jia, J. Xu and H. Song, Photocatalytic H_2O_2 Generation Reaction with a Benchmark Rate at Air‐Liquid‐Solid Joint Interfaces, *Adv. Mater.*, 2023, **36**, 2307967.

14 H. Ming, P. Zhang, Y. Yang, Y. Zou, C. Yang, Y. Hou, K. Ding, J. Zhang and X. Wang, Tailored poly-heptazine units in carbon nitride for activating peroxymonosulfate to degrade organic contaminants with visible light, *Appl. Catal., B*, 2022, **311**, 121341.

15 H. Ou, S. Ning, P. Zhu, S. Chen, A. Han, Q. Kang, Z. Hu, J. Ye, D. Wang and Y. Li, Carbon Nitride Photocatalysts with Integrated Oxidation and Reduction Atomic Active Centers for Improved CO_2 Conversion, *Angew. Chem. Int. Ed.*, 2022, **61**, e202206579.

16 Y. Li, T. Kong and S. Shen, Artificial Photosynthesis with Polymeric Carbon Nitride: When Meeting Metal Nanoparticles, Single Atoms, and Molecular Complexes, *Small*, 2019, **15**, 1900772.

17 W. Hou, H. Guo, M. Wu and L. Wang, Amide Covalent Bonding Engineering in Heterojunction for Efficient Solar-Driven CO_2 Reduction, *ACS Nano*, 2023, **17**, 20560-20569.

18 C. Feng, L. Tang, Y. Deng, J. Wang, J. Luo, Y. Liu, X. Ouyang, H. Yang, J. Yu and J. Wang, Synthesis of Leaf-Vein-Like g-C_3N_4 with Tunable Band Structures and Charge Transfer Properties for Selective Photocatalytic H_2O_2 Evolution, *Adv. Funct. Mater.*, 2020, **30**, 2001922.

19 H. Guo, L. Zhou, K. Huang, Y. Li, W. Hou, H. Liao, C. Lian, S. Yang, D. Wu, Z. Lei, Z. Liu and L. Wang, Nitrogen-Rich Carbon Dot-Mediated $n\rightarrow\pi^*$ Electronic Transition in Carbon Nitride for Superior Photocatalytic Hydrogen Peroxide Production, *Adv. Funct. Mater.*, 2024, **34**, 2402650.

20 Y. Chen, B. Zhang, Y. Liu, J. Chen, H. Pan and W. Sun, Graphitic carbon nitride-based electrocatalysts for energy applications, *Materials Today Catalysis*, 2023, **1**, 100003.

21 Z. Li, Y. Chen, Y. Guo, Y. Wang, T. Guan, J. Bai, D. Hu, H. Li and J. Du, Preparation of ultra-thin porous

carbon nitride and its photocatalytic H_2O_2 production and photodegradation of RhB, *Appl. Surf. Sci.*, 2022, **598**, 153866.
22 D. Jin, D. He, Y. Lv, K. Zhang, Z. Zhang, H. Yang, C. Liu, J. Qu and Y.-n. Zhang, Preparation of metal-free BP/CN photocatalyst with enhanced ability for photocatalytic tetracycline degradation, *Chemosphere*, 2022, **290**, 133317.
23 Y. Yang, C. Zhang, D. Huang, G. Zeng, J. Huang, C. Lai, C. Zhou, W. Wang, H. Guo, W. Xue, R. Deng, M. Cheng and W. Xiong, Boron nitride quantum dots decorated ultrathin porous g-C_3N_4: Intensified exciton dissociation and charge transfer for promoting visible-light-driven molecular oxygen activation, *Appl. Catal., B*, 2019, **245**, 87-99.
24 Z. Li, H. Lv, K. Tong, Y. He, C. Zhai, Y. Yun and M. Zhu, Modulating the precursors of carbon nitride to boost local electron delocalization for H_2O_2 photosynthesis to remove oxytetracycline and its antibiotic resistant genes, *Appl. Catal., B*, 2024, **345**, 123690.
25 J. Li, Y. Mei, S. Ma, Q. Yang, B. Jiang, B. Xin, T. Yao and J. Wu, Internal-electric-field induced high efficient type-I heterojunction in photocatalysis-self-Fenton reaction: Enhanced H_2O_2 yield, utilization efficiency and degradation performance, *J. Colloid Interface Sci.*, 2022, **608**, 2075-2087.
26 J. Hu, C. Chen, T. Hu, J. Li, H. Lu, Y. Zheng, X. Yang, C. Guo and C. M. Li, Metal-free heterojunction of black phosphorus/oxygen-enriched porous g-C_3N_4 as an efficient photocatalyst for Fenton-like cascade water purification, *J. Mater. Chem. A*, 2020, **8**, 19484-19492.
27 J. Hu, P. Zhang, T. Yang, Y. Cai, J. Qu and X. Yang, Screen superior ultra-thin g-C3N4 material for photocatalytic in-situ H_2O_2 production to remove tetracycline, *Appl. Surf. Sci.*, 2022, **576**, 151841.
28 D. Li, C. Wen, J. Huang, J. Zhong, P. Chen, H. Liu, Z. Wang, Y. Liu, W. Lv and G. Liu, High-efficiency ultrathin porous phosphorus-doped graphitic carbon nitride nanosheet photocatalyst for energy production and environmental remediation, *Appl. Catal., B*, 2022, **307**, 121099.
29 Q. Zhang, L. Li, Q. Zhou, H. Zhang, H. Zhang, B. An, H. Ning, T. Xing, M. Wang, M. Wu and W. Wu, Boosting C3H6 Epoxidation via Tandem Photocatalytic H_2O_2 Production over Nitrogen-Vacancy Carbon Nitride, *ACS Catal.*, 2023, **13**, 13101-13110.
30 Y.-Z. Zhang, C. Liang, H.-P. Feng and W. Liu, Nickel single atoms anchored on ultrathin carbon nitride for selective hydrogen peroxide generation with enhanced photocatalytic activity, *Chem. Eng. J.*, 2022, **446**, 137379.
31 C. Xue, P. Wang, H. Che, W. Liu, B. Liu and Y. Ao, Simultaneous organic pollutant degradation and hydrogen peroxide production by molecular-engineered carbon nitride, *Appl. Catal., B*, 2024, **340**, 123259.